Journal of Physics D: Applied Physics

PAPER

Localized interface modes in one-dimensional hyperuniform acoustic materials

To cite this article: S M Kuznetsova *et al* 2021 *J. Phys. D: Appl. Phys.* **54** 315303

IOP Publishing Journal of Physics D: Applied Physics
J. Phys. D: Appl. Phys. **54** (2021) 315303 (9pp) https://doi.org/10.1088/1361-6463/ac006d

Localized interface modes in one-dimensional hyperuniform acoustic materials

S M Kuznetsova[1,*], J-P Groby[1], L M García-Raffi[2] and V Romero-García[1]

[1] Laboratoire d'Acoustique de l'Université du Mans (LAUM), UMR CNRS 6613, Institut d'Acoustique–Graduate School (IA-GS), CNRS, Le Mans Université, Avenue Olivier Messiaen, 72085 Le Mans, France
[2] Instituto Universitario de Matemática Pura y Aplicada (IUMPA), Universitat Politècnica de València, Camino de Vera s/n, 46022 València, Spain

E-mail: smkuznetsova1@gmail.com

Received 18 December 2020, revised 1 March 2021
Accepted for publication 12 May 2021
Published 28 May 2021

Abstract

We theoretically, numerically and experimentally report the localization of an acoustic wave at the interface between two one-dimensional hyperuniform materials of different geometrical representations. These materials suppress the acoustic scattering in the long wavelength regime, being rather disordered and degenerate, while possessing a wide band gap. In this work, these hyperuniform materials are made of an air-filled acoustic waveguide with rigid diaphragms acting as scatterers. A wide band gap and the emergence of the edge modes provide promising applications in wave control devices.

Keywords: hyperuniform materials, localized edge states, phononic crystals, acoustics

(Some figures may appear in colour only in the online journal)

1. Introduction

Localized edge modes occurring at the connection between two materials yielding in different topological phases have long attracted attention due to their potential applications for robust transport of different types of waves. The eigenfrequencies of such boundary modes lie inside the band gap flanked by allowed bands. Translational symmetry is of crucial importance for both the existence of the band gaps and the introduction of bulk topological invariants of the system. In this regard, the topological properties are traditionally attributed to ordered materials. The emergence of the boundary modes is governed by the bulk-boundary correspondence, which is a relation between the eigenstates of the system within the bulk spectrum and the number of the supported interface modes. These modes are topologically protected, i.e. they are stable against adiabatic chiral symmetry preserving perturbations if the band gap remains open [8, 22]. The topological state of the system can be controlled by the gap closing and reopening, which is driven by the geometrical parameters.

One of the most established and common one-dimensional (1D) systems to describe topological edge states is the Su–Schrieffer–Heeger (SSH) model [27]. This model is widely used to predict and investigate the localized boundary modes in binary waveguide arrays [6], diatomic chains of plasmonic particles [16], dielectric microwave resonators [24], spins [11], etc. Topology has recently enriched the fields of acoustics and mechanics by introducing various classical analogs of quantum and electronic effects, such as Dirac cone dispersion, quantum Hall and spin Hall effects [17, 21, 33]. Periodic acoustic structures have been shown to undergo a topological phase transition accompanied by the emergence of the edge localized modes by means of varying the geometry of the sample [7, 10, 15, 20, 23, 31, 34]. In particular, the variation of the lengths of the unit cell components has been

* Author to whom any correspondence should be addressed.

shown to affect the topological properties of the second [31] and higher order gaps [20] in one-dimensional systems.

Meanwhile, topologically nontrivial states have been achieved not only in periodic structures. Topological edge modes have been observed in quasiperiodic structures [2], coupled resonator smartly patterned systems [3] and even in amorphous systems with randomly distributed particles [1, 9].

Lately, hyperuniform materials have emerged as promising candidates for the wave control, exhibiting transparency for a set of wavevectors in the long wavelength limit. Hyperuniform structures stand apart from conventional media exhibiting the properties of liquids (amorphous) and crystals (periodic) simultaneously—suppressing large scale density fluctuations. They are statistically isotropic with no long-range order [5, 29, 30]. They were found to possess wide isotropic bandgaps both in photonic [18, 19] and phononic [13] systems, in spite of being highly disordered and degenerate. These materials thus offer remarkable capabilities for engineering waveguiding devices. The band gap formation is attributed to the interplay of the hyperuniformity and the reminiscences of crystallinity always present due to the constraints imposed on the system [12]. Since the band gap closing and reopening can be achieved by varying the geometric parameters of the hyperuniform material similarly to the periodic systems, the crucial changes in the bulk eigenstates can be undergone.

In this work, we theoretically and numerically predict and experimentally observe the wave localization at the interface between two hyperuniform materials both possessing a band gap in similar ranges of frequencies. This counter-intuitive result shows the possibility of localizing waves in a controlled manner between two disordered systems due to the reminiscence of periodicity in the hyperuniform materials. To obtain a hyperuniform structure, we utilize the optimization procedure described in reference [25]. The extracted hyperuniform point distribution is used to manufacture a 1D hyperuniform material made of an air-filled waveguide of circular cross-section in which the hyperuniform distribution of rigid diaphragms is embedded. Wave propagation is numerically analyzed and experimentally validated showing good agreement. By changing the geometry of the diaphragms, the band gap closing and reopening is achieved and two complementary configurations at the opposite sides of the band gap closing are obtained. These two systems are then connected to analyze the possible localization of the acoustic wave at the interfaces between these two hyperuniform media. We also revisit the periodic counterpart of the localized edge states in periodic media from a theoretical and experimental points of view.

2. Hyperuniform materials

Consider a 1D distribution of N identical scatterers located at positions x_j which form a unit cell of size L that is periodically repeated along the x-coordinate. The reciprocal counterpart of this complex lattice is given by the reciprocal lattice vector $G = 2\pi m/L$, $m \in \mathbb{Z}$. In case of negligible interactions between the scatterers, such systems can be described by the structure factor $S(G)$

$$S(G) = \frac{1}{N}\left|\sum_{j=1}^{N} \mathrm{e}^{\mathrm{i}Gx_j}\right|^2. \tag{1}$$

The system is hyperuniform if the long-range density fluctuations are suppressed leading to vanishing structure factor $S(|G| < K) = 0$ in the vicinity of the origin of the reciprocal space with $K = 2\pi n/L$, $n \in \mathbb{N}$. The hyperuniform patterns are also characterized by the parameter χ, which defines a relative number of the independent reciprocal lattice vectors lying in the region $|G| < K$. For 1D systems, $\chi = n/N$. When $\chi \geq 0.5$, the pattern becomes crystalline, because crystal becomes the only way to meet the requirement of minimum value of the structure factor [12]. In the limit $\chi \to 0$, the configurations are disordered and represent an ideal gas, since there is no constraint anymore on the reciprocal lattice vectors [30]. In the intermediate regime, $0 < \chi < 0.5$ the configurations are disordered, although they still display some hints of crystallinity, such as reminiscences of the Bragg peaks [12] leading to isotropic gaps in the transmission spectrum. Thus, the introduction of χ as an order measure illustrates that states of matter exist between crystals and ideal gases with counter-intuitive physical properties.

To design the hyperuniform pattern, we use an optimization procedure, which looks for the positions of point scatterers x_j that minimize the structure factor for a target region $|G| < K$ as described in reference [25]. The algorithm provides a certain configuration starting from a random distribution satisfying the constraint that the particles cannot overlap ($|x_i - x_j| \geq l$ with l being the size of the particle), so that the *a posteriori* experimental validation should be performed. The objective functions to be simultaneously minimized are the structure factor

$$\phi(x_1, \ldots x_N) = \sum_{|G|<K} S(G), \tag{2}$$

and the standard deviation function

$$\sigma = \sqrt{\left|\frac{1}{N-1}\sum_{|G|<K}\left|S(G) - \frac{1}{N}\sum_{|G|<K} S(G)\right|^2\right.}. \tag{3}$$

We focus on the single unit supercell of the hyperuniform sample with $\chi = 0.2$ to ensure a high degree of disorder in the structure. Studying a single unit supercell is sufficient to represent a hyperuniform material in 1D systems. With such moderate value of χ, the area of suppressed structure factor ($f \leq 680$ Hz) is small and the material is closer to a disordered material than to a periodic one. Nevertheless, the constraint on the minimum distance between the scatterers introduces a

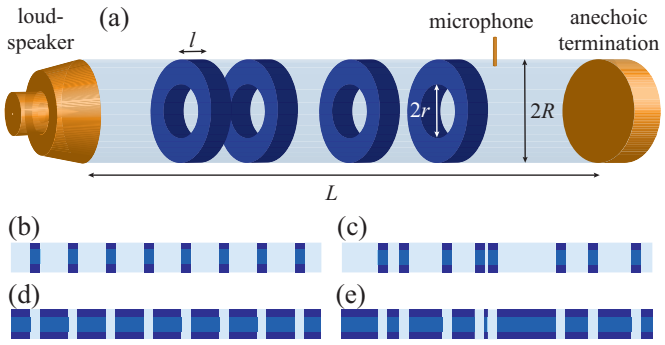

Figure 1. (a) Schematic view of the experimental setup, (b), (d) longitudinal section of the positive and negative periodic waveguides, respectively, (c), (e) longitudinal section of the positive and negative hyperuniform waveguides, respectively. The dark blue regions correspond to the diaphragms and the light blue regions correspond to the empty spaces inside the waveguide.

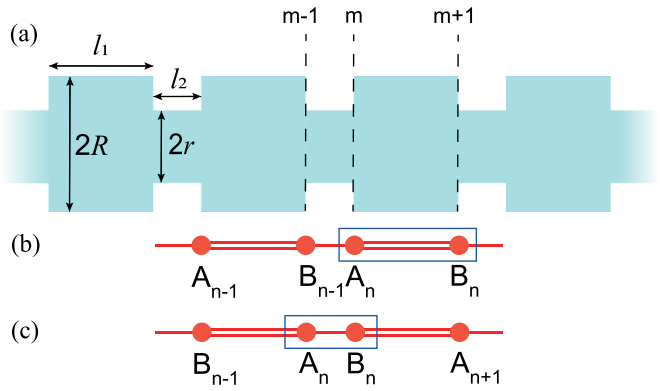

Figure 2. (a) Scheme of a 1D waveguide of radius R with diaphragms of radius r and length l_2, (b), (c) corresponding SSH-like chains of point particles of type A and B with different choices of a unit cell $[AB]$.

short-range correlation and leads to the reminiscences of crystallinity of the system, which will be discussed in the following sections.

3. Experimental setup

The setup utilized in this work is made of a main waveguide of radius R in which diaphragms with inner radius $r < R$ act as the scatterers of the system. N diaphragms located at the specific positions provided by the optimization procedure will constitute the whole system (see appendix A for the exact positions). A scheme of the setup is shown in figure 1. The dimensions are chosen to satisfy the single mode propagation regime in the frequency range of interest, i.e. the range of frequencies analyzed in the setup are always smaller than the cutoff frequency of the waveguide. The radius of the waveguide is $R = 1.5$ cm and its length is $L = 1$ m. The hyperuniform material supercell is optimized considering $N = 20$ scatterers. The radii of the diaphragms are chosen identical $r = R/2$ in order to open the band gap of the hyperuniform material. A plexiglass tube and PVC diaphragms were used in the experiments. Both materials are considered acoustically rigid due to their large impedance mismatch with respect to that of the air. A loudspeaker was used to generate a plane wave at one end of the plexiglass tube and a single microphone was used to measure the amplitude of the pressure field at the desired locations. At the opposite end of the tube, an anechoic termination with less than 5% of reflection amplitude in the analyzed frequency range was used.

In this work, we consider either a periodic or a hyperuniform distributions of scatterers represented by two configurations residing in different states. We introduce the variable radii $r'(t) = R/2(1+t)$, $R'^{(t)} = R(1-t/2)$ and the parameter $t \in [0, 1]$ for the simulation of the band gap closing and reopening. Two complementary configurations referred to as the positive and the negative configurations are obtained by varying t from 0 to 1 (see figures 1(c) and (e)). They stay at different states, i.e. the positive configuration stays on the left of the band gap closing with $t < 0.5$ while the negative one stays on the right of the band gap closing with $t > 0.5$.

In practice, the positive configuration is realized by locating the diaphragms of length $l = 1.5$ cm at the scatterers positions of the hyperuniform point pattern, while the negative configuration is realized by locating the different diaphragms between the scatterers positions. These two configurations with $t = 0$ and $t = 1$ are used in the experiments.

The same concept is applied to the periodic system. The positive and the negative periodic waveguides with five inserted diaphragms are considered. Two types of diaphragms were fabricated—the first type of lengths $l_2 = 1.5$ cm and the second type of lengths $l_2 = 3.5$ cm—for the construction of the periodic waveguides. The size of the constituent unit cell in both configurations is fixed to $d = l_1 + l_2 = 5$ cm. In this way, the two configurations are complementary to each other (see figures 1(b) and (d)). The periodic structure made of the diaphragms of length $l_2 = 1.5$ cm is referred to as positive configuration, while that made of the diaphragms of length $l_2 = 3.5$ cm is referred to as the negative configuration.

4. Revising the localized modes in 1D periodic systems

4.1. Characteristics of 1D periodic materials

A 1D crystalline scatterers distribution is implemented by periodically embedding diaphragms of radii $r = R/2$ and length l_2 acting as scatterers in an air-filled waveguide of radius R (figure 2(a)). Only plane acoustic waves are assumed to propagate.

The pressure p and the acoustic flow u at two points (initial i and final f) along the waveguide are related via the transfer matrix T

$$\begin{pmatrix} p_i \\ u_i \end{pmatrix} = T \begin{pmatrix} p_f \\ u_f \end{pmatrix}, \tag{4}$$

where T is the product of all the intermediate transfer matrices along the $i \to f$ path

$$T = \prod_{j=1}^{N} T_j. \tag{5}$$

The transfer matrix of a waveguide or a diaphragm of the length l_j, cross section S_j and reduced impedance $Z_j = \rho c / S_j$ is

$$T_j = \begin{pmatrix} \cos(kl_j) & \imath Z_j \sin(kl_j) \\ \frac{\imath}{Z_j}\sin(kl_j) & \cos(kl_j) \end{pmatrix}, \tag{6}$$

where k is a wavenumber and the $e^{-i\omega t}$ time harmonic dependence is assumed. The flow in the final point is obtained from equation (4)

$$u_f = V_{i,f}\, p_f + W_{i,f}\, p_i, \tag{7}$$

where $V_{i,f} = -\frac{T_{11}}{T_{12}}$, $W_{i,f} = \frac{1}{T_{12}}$. Considering the acoustic flows from the points $(m+1)$ and $(m-1)$ into the point m, we obtain

$$(V_{m-1,m} + V_{m+1,m})p_m = -W_{m-1,m}p_{m-1} - W_{m+1,m}p_{m+1}. \tag{8}$$

The opposite signs of flows coming from opposite directions (from the points $m+1$ and $m-1$) into the point m have been accounted for.

Let us refer to the junctions with a large radius part at the right as the A-junctions and those with a large radius part at the left as the B-junctions (figure 2(b)). If $l_1 = l_2 = l$, equation (8) takes the form of a pair of SSH equations

$$\begin{aligned} \varepsilon A_n &= \kappa_2 B_{n-1} + \kappa_1 B_n, \\ \varepsilon B_n &= \kappa_2 A_{n+1} + \kappa_1 A_n, \end{aligned} \tag{9}$$

where A_n, B_n represent the pressures at the corresponding junctions, $\varepsilon = \cos(kl)$, $\kappa_1 = \frac{R^2}{r^2+R^2}$, and $\kappa_2 = \frac{r^2}{r^2+R^2}$. The junctions are now identified to the particles in a dimer chain of the original SSH model with a unit cell $[AB]$. According to the expressions of the coupling coefficients $\kappa_{1,2}$, the parts of the tube with radii R and r correspond to the strong and weak couplings between the particles. Thus, the region between the junctions A_n and B_n of a waveguide plays the role of the unit cell and the region between the junctions B_n and A_{n+1} plays the role of the connection between the unit cells. Another unit cell can be chosen, as that depicted in figure 2(c), which would lead to the same system of equation but with interchanged coupling coefficients κ_1 and κ_2.

The dispersion relation of the SSH system exhibits a gap $\Delta\varepsilon = |\kappa_1 - \kappa_2|$. When $\kappa_1 = \kappa_2$ the gap closes and the eigenstates of the system with arbitrarily small eigenvalues are allowed propagating modes. The condition $\kappa_1 = \kappa_2$ corresponds to $R = r$, i.e. the empty tube. If the system is finite $(n = 1, \ldots, N)$, it may support zero-eigenvalue states. Assuming $\varepsilon = 0$ in equation (9), the solution becomes

$$\begin{pmatrix} A_n \\ B_n \end{pmatrix} = (-1)^{n-1} \left(\frac{\kappa_1}{\kappa_2}\right)^{n-1} \begin{pmatrix} A_1 \\ 0 \end{pmatrix}, \tag{10}$$

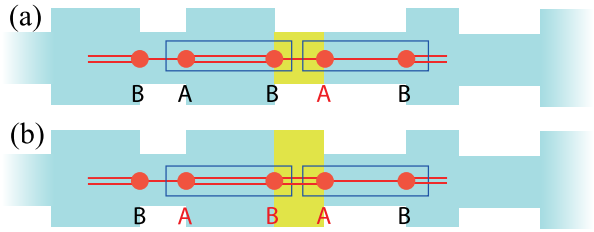

Figure 3. (a) A monomer and (b) a trimer defects between two periodic waveguides and the corresponding SSH-like particle chains.

$$\begin{pmatrix} A_n \\ B_n \end{pmatrix} = (-1)^{n-1} \left(\frac{\kappa_2}{\kappa_1}\right)^{n-1} \begin{pmatrix} 0 \\ B_1 \end{pmatrix}. \tag{11}$$

Having an eigenfrequency inside the band gap, the solutions should be localized at the sites A_1 and B_N. This requirement is fulfilled if the inter-cell coupling κ_2 is stronger than the intra-cell one κ_1. Otherwise, the solutions are delocalized and should be disregarded. The localized edge states are topologically protected. They remain present under the adiabatic modifications of the parameters (continuous modifications preserving the chiral symmetry inherent to this system [4] and the open band gap). The case $\kappa_2 > \kappa_1$ is qualified as topological, while the opposite one is trivial.

Now, we consider the waveguide with different lengths of the diaphragms and the empty spaces ($l_1 \neq l_2$). The system is thus described by modified equations. However, the chiral symmetry is preserved and the system presents the features similar to those of the SSH model in terms of the band structure and emergence of interface states.

The localized edge states appear not only at the edges of the chain, but also at the interface between the two phases—the trivial and topological ones. There are two ways to connect two finite structures of different topological phases—via weak (figure 3(a)) or strong (figure 3(b)) coupling [6]. The former is a monomer defect and the later is a trimer defect, represented by a particle A and particles ABA written in red in figures 3(a) and (b), respectively. When $l_1 = l_2$ a monomer defect supports a localized mode with a maximum amplitude at the defect particle A, while the trimer defect supports a localized mode with a node at the defect center B [6, 10]. When $l_1 \neq l_2$ the similar behaviour of the interface modes is expected.

4.2. Observation of the localized interface modes in periodic systems

We consider a 1D crystalline scatterers distribution with $l_1 \neq l_2$. In figure 4(a), we plot the dispersion relation of the positive (red dots) and the negative (blue dots) configurations. If R and r are continuously interchanged, the band gap closes and reopens (see the inset in figure 4(a), where the lower and upper edge bands of the band gap of the different configurations at $dk = \pi$ are represented). The transmission coefficients of these finite configurations are plotted in figures 4(b) and (c). The region with transmission suppression corresponds to the position of the band gap predicted by the dispersion relation.

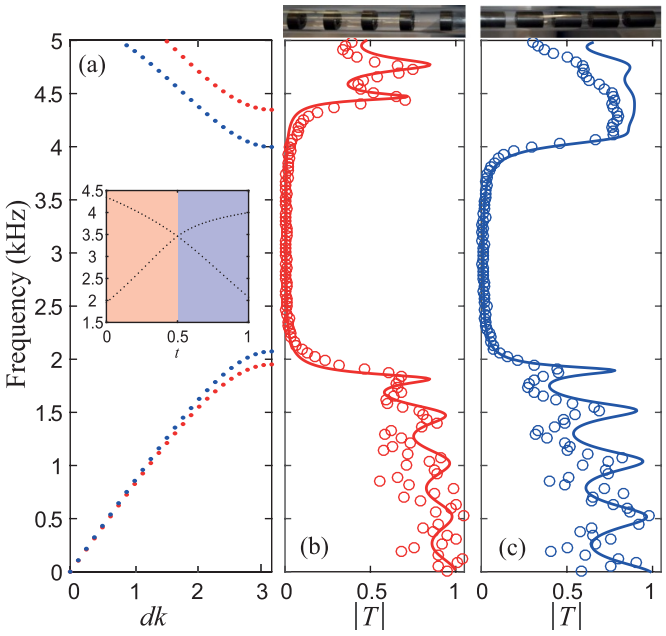

Figure 4. (a) Dispersion diagram of a periodic waveguide in positive (red dotted line) and negative (blue dotted line) configurations, the band gap closing and reopening is shown on the inset, (b), (c) transmission coefficients of the positive and negative cases respectively. The solid lines correspond to the calculations and the circles correspond to the experimental results.

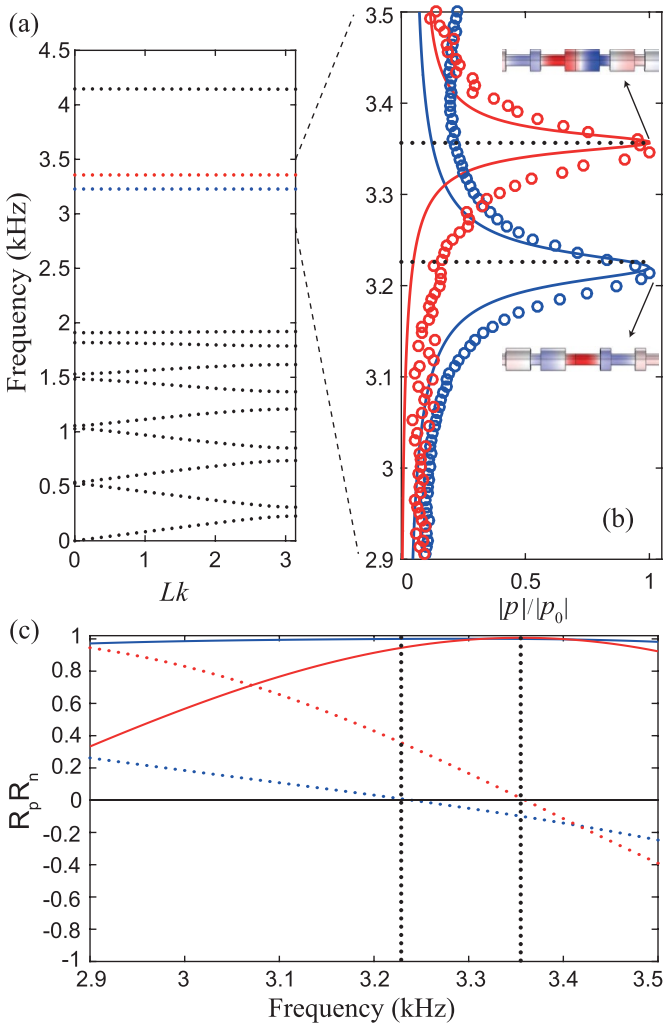

Figure 5. (a) Dispersion diagram of connected positive and negative periodic waveguides, (b) normalized pressure amplitude at the connection between the positive and negative waveguides measured with respect to the amplitude inside an empty tube p_0. The red line corresponds to the strong connection and the blue line corresponds to the weak connection. The circles represent the experimental results. The insets represent pressure distributions in the corresponding modes, (c) Re(R_pR_n) (solid lines) and Im(R_pR_n) (dotted lines) as functions of frequency for strong (red) and weak (blue) connection of two periodic waveguides. Black dotted lines correspond to the expected frequencies from the dispersion diagram.

The equidistant peaks outside the band gap are attributed to the Fabry–Perot resonances of a finite waveguide.

Since the connection of two materials in different topological phases supports a localized interface mode in the SSH model, we expect the same behavior in our periodic structures. In order to analyze the effect of the localized modes in the dispersion relation, we have to consider a new supercell made of the combination of a positive and a negative supercells in which the defect is in the middle, as it is usually done in the literature [6, 23]. Thus we consider a supercell consisting of the connection of a positive and a negative supercells with five periods in each, being enough distance to avoid the coupling between the localized modes due to the periodicity of the supercell. Indeed, two localized modes inside a band gap with a flat dispersion, corresponding to two types of connection between the waveguides—weak and strong ones—are encountered in the dispersion diagram depicted in figure 5(a). The weak connection supports a lower frequency mode, with a symmetric pressure profile relative to the connection point. The strong connection maintains a higher frequency mode with an antisymmetric profile. In figure 5(b), we plot the normalized pressure amplitudes at the connection between the two waveguides coupled in the two described ways: red (blue) lines and symbols correspond to the strong (weak) connection supporting an antisymmetric (a symmetric) mode. In the insets of figure 5(b), we plot the pressure field distributions (the real parts) of the interface modes showing the symmetry of each interface mode. The experimental measurements are shown as circles and appear to be in a good agreement with the predictions. The black lines represent the expected interface modes frequencies from the dispersion diagram that match the experimental peaks.

Surface modes at the interface between two materials of surface impedances Z_1 and Z_2 appear as the poles of the reflection coefficient $R_{12} = \frac{Z_1 - Z_2}{Z_1 + Z_2}$. For photonic [14] and phononic [20, 32] crystals, $Z_{1,2}$ are related to the topological invariants of the corresponding materials. The equality

$$Z_1 + Z_2 = 0, \tag{12}$$

is thus a condition for the emergence of the topologically protected interface states. Different signs of the surface impedances indicate that the two connected materials reside in different topological phases. The surface impedance of the

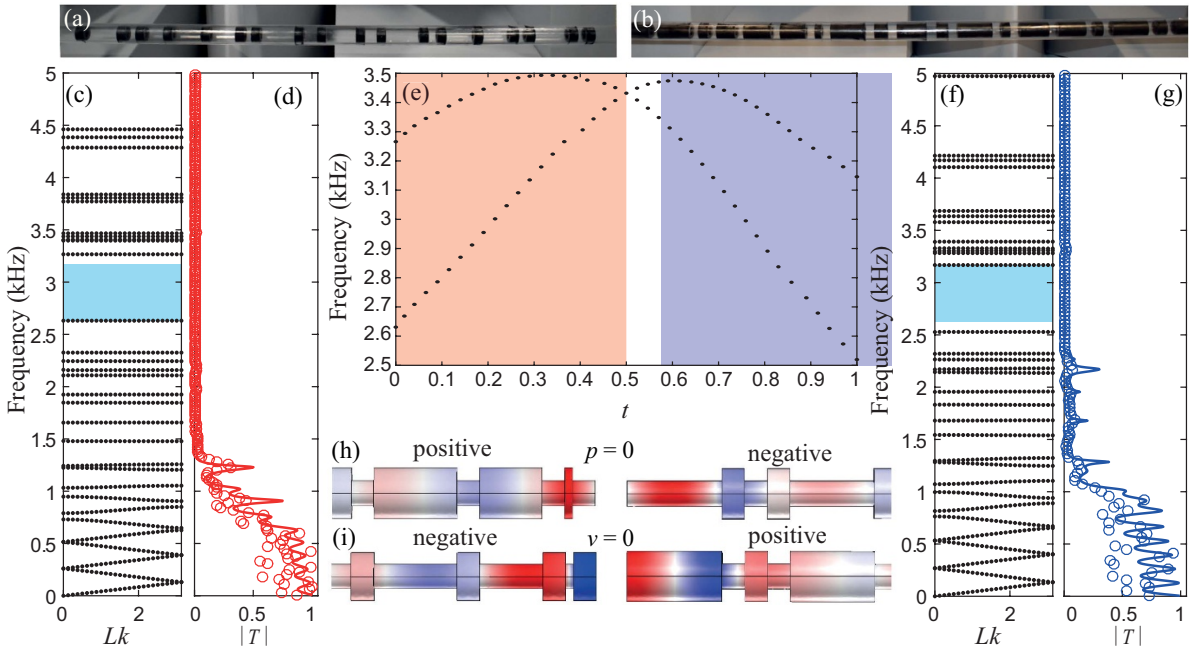

Figure 6. (a) Positive and (b) negative waveguides designed upon a hyperuniform scatterers distribution, (c), (d) dispersion diagram and the transmission coefficient of a positive waveguide, (e) closing of the band gap of a hyperuniform material with the variation of the waveguide and diaphragms radii, the red region corresponds to the positive waveguide, the blue region corresponds to the negative one, (f), (g) dispersion diagram and the transmission coefficient of a negative waveguide, (h), (i) pressure profiles in the edge modes of single positive and negative waveguides for Dirichlet and Neumann boundary conditions.

material can be obtained by measuring the reflection coefficient at its interface with air $Z_{1,2} = Z_0 \frac{1+R_{1,2}}{1-R_{1,2}}$, where Z_0 is the impedance of air. Thus, the equation equation (12) reduces to the requirement [20, 32]

$$\begin{aligned} \Re(R_1 R_2) &= 1, \\ \Im(R_1 R_2) &= 0. \end{aligned} \tag{13}$$

Figure 5(c) illustrates the product of the reflection coefficients from the single positive and negative waveguides $R_p R_n$ at the ends, which form a strong (read line) and a weak (blue line) connections. The frequencies satisfying equation (13) perfectly match the frequencies of the localized modes identified in the dispersion diagram (black dotted lines). Thus, the red and blue regions on the inset in figure 4(a) correspond to different topological phases.

5. Properties of the hyperuniform materials: closing and reopening band gap

5.1. Characteristics of the 1D hyperuniform materials

We first analyze both the dispersion relation and the transmission through the system. Figure 6(a) shows the distribution of scatterers in the designed positive hyperuniform material and figure 6(c) depicts its dispersion relation. Several flat eigenmodes, attributed to the modes localized inside the waveguide due to the disordered distribution of scatterers, are located in the band gap. These modes present a very low dispersion with small group velocity. The presence of the viscothermal losses in the system dramatically impacts them [28]. This results in a very low transmission coefficient over a broad frequency range, as shown in figure 6(d). This remarkable transmission dip is much wider than that of a periodic waveguide studied in the 4. The peaks in the transmission coefficients in the low frequency propagative regime are attributed to Fabry–Perot resonances (see appendix B).

We now focus on the blue region highlighted in the dispersion diagram in figure 6(c). It corresponds to the gap between the 20th and 21st modes, where a periodic structure consisting of 20 unit cells possesses a band gap due to the folding of the Brillouin zone. Thus, we expect to observe some reminiscence of the periodicity in this region. The width of this band gap is defined by the ratio of the radius of the diaphragm over that of the waveguide, as it can be seen from the figure 6(e), where the lower and upper edge of the band gap at $Lk = 0$ represented by the blue area in figure 6(c) are depicted. The positive and the negative configurations are shown in figures 6(a) and (b), respectively. The dispersion diagram and the transmission spectrum of the negative configuration shown in figures 6(f) and (g) respectively are similar to those of the positive one. The band gap we are interested in, shown by the blue region, lies in the same frequency range as for the positive configuration.

5.2. Observation of the localized edge states in hyperuniform materials

We have revised the features of periodic structures as well as theoretically and experimentally shown in section 4 the excitation of edge modes by using periodic distribution of

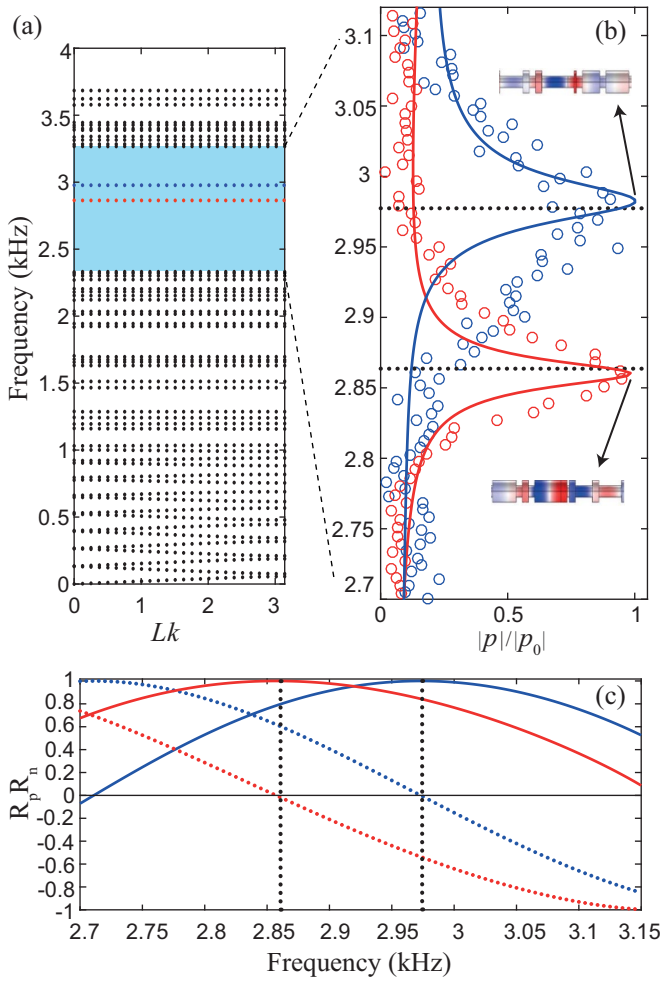

Figure 7. (a) Dispersion diagram of connected positive and negative hyperuniform waveguides, (b) normalized pressure amplitude at the connection between the positive and negative waveguides measured with respect to the amplitude inside the empty tube p_0. The red line corresponds to the strong connection and the blue line corresponds to the weak one, the circles represent the experimental results, (c) Re(R_pR_n) (solid lines) and Im(R_pR_n) (dotted lines) for strong (red) and weak (blue) connection. Black dotted lines correspond to the expected frequencies from the dispersion diagram.

scatterers in our setup. In this work, although we study a disordered system, periodicity related features still remain. Thus, we expect to observe the reminiscences of the topologically protected states at the interface between a positive and a negative hyperuniform materials. To do that we proceed as in the periodic case by considering a supercell made of the connection of a positive and a negative supercells allowing us to analyze the effect of the localized modes in the dispersion relation.

Both positive and negative waveguides under consideration possess localized edge modes with frequencies inside the band-gap. Their profiles are shown in figures 6(h) and (i) for the two types of boundary condition—Dirichlet ($p = 0$) and Neumann ($v = 0$), respectively.

The positive and negative waveguides can be connected in two ways—either by means of the ends of a larger radius (referred to as the strong connection), or by means of the ends of a smaller radius (referred to as the weak connection). We notice the localized interface modes inside the band gap, as shown in the dispersion relation in figure 7(a). The mode profiles are shown on the insets of figure 7(b) next to the corresponding normalized pressure amplitudes measured at the connection. The numerical prediction (continuous line) and the experimental results (symbols) are in good agreement. The reminiscences of the symmetric and antisymmetric behavior of Re(p) of the field of these modes, which is inherent in the periodic case, are visible. The frequencies of the interface modes are in good agreement with the predictions of the dispersion relation.

We evaluated numerically the reflection coefficients of the single positive (R_p) and negative (R_n) hyperuniform materials at their right and left ends, in order to account for both types of connections, considering a single unit supercell. Due to the fact that we are in the band gap region, that we are considering a 1D system, and that at this particular frequency the reflection coefficient is maximal, the recovered impedance is that of the semi-infinite medium. The scattering coefficients are obtained from the pressure evaluated at two points upstream and downstream the material [26]. The real and imaginary parts of R_pR_n are shown in figure 7(c) in solid and dotted lines, respectively. The frequencies, where the equation (13) is satisfied, perfectly match those of the localized modes in the dispersion diagram (vertical black dotted lines). Thus, the red and blue regions in figure 6(e) correspond to the reminiscences of different topological phases inherent to periodic structures.

6. Conclusion

In this work, we have implemented a previously developed approach [25] to engineer a 1D hyperuniform material, which possesses extremely broad band transmission suppression. The system was analyzed numerically and experimentally and consists in a waveguide with rigid diaphragms embedded in. Interchanging the locations of the diaphragms and the empty spaces, we reach a transition point, which resembles the topological phase transition occurring in the periodic systems. Despite the system is disordered, connecting two waveguides yielding on opposite sides from this point leads to an emergence of localized interface modes. Their profiles are similar to those of the periodic waveguides. Thus, we observe the reminiscences of non-trivial topological behavior of periodic structures in the disordered system.

Data availability statement

The data that support the findings of this study are available upon reasonable request from the authors.

Acknowledgments

This work has been funded by the project HYPERMETA funded under the program Étoiles Montantes of the Région Pays de la Loire as well as by the ANR-RGC METARoom (ANR-18-CE08-0021) project.

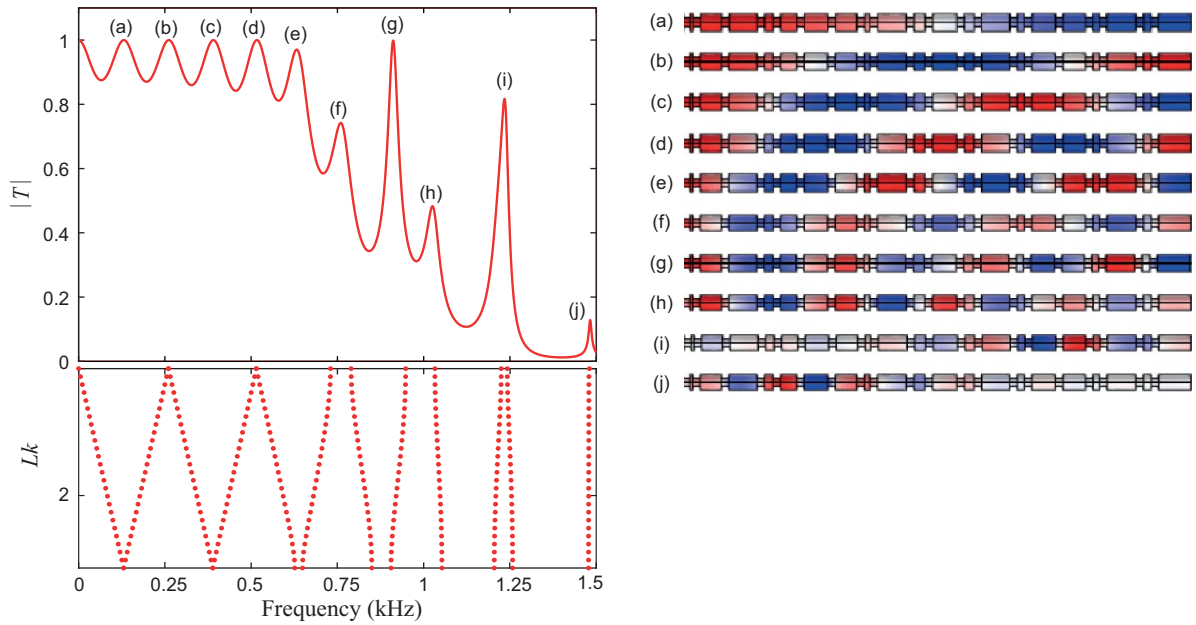

Figure B1. Transmission coefficient, dispersion relation and and the pressure profiles (real parts) of the low-frequency Fabry–Perot resonances of the positive hyperuniform waveguide.

Appendix A. Diaphragms positions in a hyperuniform waveguide

Positions of the left edges of the diaphragms in the positive hyperuniform configuration are as follows: [0 0.020 0.077 0.147 0.178 0.225 0.286 0.343 0.369 0.440 0.477 0.540 0.574 0.644 0.673 0.734 0.793 0.820 0.892 0.922] (m).

Appendix B. Low-frequency Fabry–Perot resonances

We have performed a calculation of the transmission coefficient T of the lossless positive hyperuniform material, which is shown in the figure B1 together with the dispersion diagram. The low-frequency peaks are equidistant and every following peak provides a pressure profile with an additional node as compared to the previous one (the right panel of the figure). These are the properties of the Fabry–Perot resonances. In addition, from the dispersion diagram one can calculate the velocity of approximately 260.7 m s^{-1}. Inserting this value into the condition of the Fabry–Perot resonances $Lk = n\pi$ one obtains a resonance frequency difference of approximately 130.35 Hz, which equals to the distance between the low-frequency peaks. As the speed of sound reduces with the increase of frequency due to the dispersion, the higher-frequency peaks are farther apart. The modes corresponding to the peaks (f) and (h) are attenuated because of their location inside a band gap. The higher-order modes (i) and (j) are localized inside the waveguide and have a rather small velocity corresponding to the localized modes.

ORCID iDs

S M Kuznetsova https://orcid.org/0000-0002-4773-1308
J-P Groby https://orcid.org/0000-0002-9308-8261
L M García-Raffi https://orcid.org/0000-0003-3985-8453
V Romero-García https://orcid.org/0000-0002-3798-6454

References

[1] Agarwala A and Shenoy V B 2017 Topological insulators in amorphous systems *Phys. Rev. Lett.* **118** 236402
[2] Apigo D J, Cheng W, Dobiszewski K F, Prodan E and Prodan C 2019 Observation of topological edge modes in a quasiperiodic acoustic waveguide *Phys. Rev. Lett.* **122** 095501
[3] Apigo D J, Qian K, Prodan C and Prodan E 2018 Topological edge modes by smart patterning *Phys. Rev. Materials* **2** 124203
[4] Asbóth J, Oroszlány L and Pályi A 2016 Lecture Notes in Physics *A Short Course on Topological Insulators: Band Structure and Edge States in One and Two Dimensions* (Berlin: Springer) **919** 166
[5] Batten R D, Stillinger F H and Torquato S 2008 Classical disordered ground states: super-ideal gases and stealth and equi-luminous materials *J. Appl. Phys.* **104** 033504
[6] Blanco-Redondo A, Andonegui I, Collins M J, Harari G, Lumer Y, Rechtsman M C, Eggleton B J and Segev M 2016 Topological optical waveguiding in silicon and the transition between topological and trivial defect states *Phys. Rev. Lett.* **116** 163901
[7] Brendel C, Peano V, Painter O and Marquardt F 2017 Snowflake topological insulator for sound waves (arXiv:1701.06330)

[8] Chen B-H and Chiou D-W 2020 An elementary rigorous proof of bulk-boundary correspondence in the generalized Su-Schrieffer-Heeger model *Phys. Lett.* A **384** 126168
[9] Costa M, Schleder G R, Buongiorno Nardelli M, Lewenkopf C and Fazzio A 2019 Toward realistic amorphous topological insulators *Nano Lett.* **19** 8941–6
[10] Esmann M, Lamberti F R, Lemaître A and Lanzillotti-Kimura N D 2018 Topological acoustics in coupled nanocavity arrays *Phys. Rev.* B **98** 161109
[11] Estarellas M P, D'Amico I and Spiller T P 2017 Topologically protected localised states in spin chains *Sci. Rep.* **7** 1–10
[12] Fan Y, Percus J K, Stillinger D K and Stillinger F H 1991 Constraints on collective density variables: one dimension *Phys. Rev.* A **44** 2394–402
[13] Gkantzounis G, Amoah T and Florescu M 2017 Hyperuniform disordered phononic structures *Phys. Rev.* B **95** 094120
[14] Lawrence F J, Botten L C, Dossou K B, McPhedran R C and de Sterke C M 2010 Photonic-crystal surface modes found from impedances *Phys. Rev.* A **82** 053840
[15] Li X, Meng Y, Wu X, Yan S, Huang Y, Wang S and Wen W 2018 Su-Schrieffer-Heeger model inspired acoustic interface states and edge states *Appl. Phys. Lett.* **113** 203501
[16] Ling C W, Xiao M, Chan C T, Yu S F and Fung K H 2015 Topological edge plasmon modes between diatomic chains of plasmonic nanoparticles *Opt. Express* **23** 2021–31
[17] Ma G, Xiao M and Chan C 2019 Topological phases in acoustic and mechanical systems *Nat. Rev. Phys.* **1** 281–94
[18] Man W *et al* 2013 Photonic band gap in isotropic hyperuniform disordered solids with low dielectric contrast *Opt. Express* **21** 19972–81
[19] Man W *et al* 2013 Isotropic band gaps and freeform waveguides observed in hyperuniform disordered photonic solids *Proc. Natl Acad. Sci.* **110** 15886–91
[20] Meng Y *et al* 2018 Designing topological interface states in phononic crystals based on the full phase diagrams *New J. Phys.* **20** 073032
[21] Mousavi S H, Khanikaev A B and Wang Z 2015 Topologically protected elastic waves in phononic metamaterials *Nat. Commun.* **6** 1–7
[22] Ozawa T *et al* 2019 Topological photonics *Rev. Mod. Phys.* **91** 015006
[23] Pal R K, Vila J, Leamy M and Ruzzene M 2018 Amplitude-dependent topological edge states in nonlinear phononic lattices *Phys. Rev.* E **97** 032209
[24] Poli C, Bellec M, Kuhl U, Mortessagne F and Schomerus H 2015 Selective enhancement of topologically induced interface states in a dielectric resonator chain *Nat. Commun.* **6** 1–5
[25] Romero-García V, Lamothe N, Theocharis G, Richoux O and García-Raffi L 2019 Stealth acoustic materials *Phys. Rev. Appl.* **11** 054076
[26] Song B and Bolton J S 2000 A transfer-matrix approach for estimating the characteristic impedance and wave numbers of limp and rigid porous materials *J. Acoust. Soc. Am.* **107** 1131–52
[27] Su W P, Schrieffer J R and Heeger A J 1979 Solitons in polyacetylene *Phys. Rev. Lett.* **42** 1698–701
[28] Theocharis G, Richoux O, Romero-García V, Merkel A and Tournat V 2014 Limits of slow sound propagation and transparency in lossy, locally resonant periodic structures *New J. Phys.* **16** 093017
[29] Torquato S 2016 Hyperuniformity and its generalizations *Phys. Rev.* E **94** 022122
[30] Torquato S, Zhang G and Stillinger F H 2015 Ensemble theory for stealthy hyperuniform disordered ground states *Phys. Rev.* X **5** 021020
[31] Xiao M, Ma G, Yang Z, Sheng P, Zhang Z and Chan C T 2015 Geometric phase and band inversion in periodic acoustic systems *Nat. Phys.* **11** 240–4
[32] Xiao M, Zhang Z Q and Chan C T 2014 Surface impedance and bulk band geometric phases in one-dimensional systems *Phys. Rev.* X **4** 021017
[33] Xie B, Liu H, Cheng H, Liu Z, Chen S and Tian J 2019 Acoustic topological transport and refraction in a Kekulé lattice *Phys. Rev. Appl.* **11** 044086
[34] Martí-Sabaté M and Torrent D 2021 Dipolar localization of waves in twisted phononic crystal plates *Phys. Rev. Appl.* **15** L011001